

Chaos and Fractals in Geodesic Motions Around a Non-Rotating Black-Hole with an External Halo

Alessandro P. S. de Moura*
Instituto de Física Gleb Wataghin, UNICAMP, Brazil

Patricio S. Letelier†
Instituto de Matemática, Estatística e Ciência da Computação, Departamento de Matemática Aplicada, UNICAMP, Brazil

We investigate the occurrence chaos in the escape of test particles moving in the field of a Schwarzschild black hole surrounded by an external halo. The motion of both material particles and zero rest mass particles is considered. The chaos is characterized by the fractal dimension of boundary between the basins of the different escapes, which is a topologically invariant characterization. We find chaos in the motion of both material particles and null geodesics.

I. INTRODUCTION

The study of chaos in dynamical systems with unbounded orbits is relatively recent [1]. The characterization of chaos for this class of problems is different from that used for bounded dynamics, which is based upon the destruction of KAM tori. One of the most important situations with unbounded motion is that of the escape of particles from a certain region; this problem is closely related to scattering, the difference between the two being essentially the choice of the initial conditions. Escapes have been studied for several systems: galactic dynamics [2], nonlinear oscillations [3,4], two-dimensional conservative mappings [5] and inflationary cosmology [6] are only a few examples.

In this paper, we study the dynamics of unbounded orbits of test particles (including zero rest mass particles) in a general-relativistic vacuum static axisymmetric system consisting of a non-rotating black hole surrounded by an external multipolar halo; in particular, we are interested in the escape properties of these systems. If a system has two or more physically well-defined escapes for a given set of parameters of the metric (for instance, regions where a particle runs away to infinity, or where it falls into an event horizon), then the escape it chooses is a function of its initial conditions; when this function has a fractal structure, we have a well-defined kind of chaos, and the correspondent fractal dimension gives a good quantitative characterization of the chaos, besides having a simple physical interpretation as a measure of the sensitivity to initial conditions (see section III). Since the fractal nature of the boundary between the escapes as well as its associated fractal dimension are topological invariants, they are independent of the choice of the space-time coordinates; this assures the meaningfulness of this characterization for General Relativity.

This paper is organized as follows: in section II we review the Weyl form of the general vacuum static axisymmetric metric and some of its properties; in section III we define the box-counting dimension and discuss its physical significance; in section IV, we investigate the basins of escape in the motion of material particles for some choices of static axisymmetric metrics, and show numerically the existence of chaos; in section V, we show that null geodesics are regular (non-chaotic) in the field of a dipolar halo (plus the black hole), but chaos arises if we add multipole moments of higher order to the halo; and in section VI we summarize our results and draw some conclusions.

II. THE WEYL METRIC

Throughout this article, we use the Weyl metric to describe a general static axisymmetric space-time [7]:

$$ds^2 = e^{2\psi} dt^2 - e^{-2\psi} [e^{2\gamma}(dr^2 + dz^2) + r^2 d\phi^2], \quad (1)$$

where r and z are the radial and axial coordinates, and ϕ is the angle about the z axis, which is the axial symmetry axis. Throughout this article, we will use units such that $c = 1$ and $m = 1$, where m is the mass of a test particle moving in spacetime (1). ψ and γ are functions of r and z only. In these coordinates, the vacuum Einstein equations reduce to:

*email: sandro@ifi.unicamp.br

†email: letelier@ime.unicamp.br

$$\Delta\psi \equiv \frac{\partial^2\psi}{\partial r^2} + \frac{1}{r}\frac{\partial\psi}{\partial r} + \frac{\partial^2\psi}{\partial z^2} = 0; \quad (2)$$

$$d\gamma = r \left[\left(\frac{\partial\psi}{\partial r} \right)^2 - \left(\frac{\partial\psi}{\partial z} \right)^2 \right] dr + 2r \frac{\partial\psi}{\partial r} \frac{\partial\psi}{\partial z} dz. \quad (3)$$

The first expression is just Laplace's equation in cylindrical coordinates; the second equation is a quadrature whose integrability is automatically guaranteed by eq.(2).

The metric (1) is independent of the time t and of the symmetry angle ϕ . From this we obtain the two constants of motion E (energy) and L_z (projection of the angular momentum on the symmetry axis), that are conserved along the trajectories of test particles in the metric (1). They are given by:

$$E \equiv p_t = g_{tt}\dot{t}; \quad (4)$$

$$L_z \equiv p_\phi = g_{\phi\phi}\dot{\phi}, \quad (5)$$

where the dot denotes differentiation with respect to an affine parameter. The only independent dynamical variables are thus r , z and their momenta p_r and p_z : the time evolution of t and ϕ are given by the quadratures above. This means that the dynamical system corresponding to the motion of test particles in the Weyl metric has only two degrees of freedom.

To proceed further, it is convenient to define the prolate spheroidal coordinates u and v by:

$$z = uv; \quad (6)$$

$$r^2 = (u^2 - 1)(1 - v^2); \quad (7)$$

$$u \geq 1; \quad -1 \leq v \leq 1.$$

In these coordinates, equation (2) is separated, and a general solution is obtained in a series of products of Legendre polynomials and zonal harmonics [8]. The solution we are interested in is:

$$\psi = \frac{1}{2} \ln \left(\frac{u-1}{u+1} \right) + \sum_{n=1}^{\infty} a_n P_n(u) P_n(v). \quad (8)$$

The first term represents a Schwarzschild black hole, and the terms under the summation sign are multipolar contributions from an external halo.

Using the coordinates u and v and the expression (8) for ψ , γ can be obtained from a straightforward integration of eq. (3); the constant of integration is chosen so as to avoid conical singularities on the z axis, by imposing $\gamma = 0$ for $r = 0$ and $|z| > 1$.

In this article, we are interested in the multipole contributions only up to the octopole term ($n = 3$ in eq.(8)). Redefining the coefficients in the expansion, we can write ψ as:

$$\begin{aligned} \psi = & \frac{1}{2} \ln \left(\frac{u-1}{u+1} \right) - Duv + (Q/6)(3u^2 - 1)(3v^2 - 1) + \\ & (O/10)uv(5u^2 - 3)(5v^2 - 3), \end{aligned} \quad (9)$$

where D , Q and O are defined as the dipole, quadrupole and octopole moments. Now an explicit expression for γ may be found by direct integration. Since the expressions are quite cumbersome and not particularly illuminating, we will not write them here; they can be found in [10,11]. We only observe that due to the nonlinearity of Einstein's equation, reflected in this case in eq. (3), there are nonlinear terms of interaction between the multipole terms in γ : the gravitational field due to the different terms in the expansion (8) is not simply the superposition of the fields due to each term separately.

We finish this discussion by observing that the coordinates u and v describe the metric only outside the black hole; in these coordinates, the event horizon is given by the segment $r = 0$, $|z| \leq 1$. Since we are interested only in the motion of particles outside the event horizon, this singular behavior of the coordinate transformation $(r, z) \rightarrow (u, v)$ will not concern us here.

III. FRACTAL BASIN BOUNDARIES

We now review briefly some basic concepts on fractals in dynamical systems with escapes; a complete discussion is found in [1].

In order to simplify the discussion, we will suppose we have a region in the phase space of the system (denoted the *inner region*) which has two distinct escapes, denoted by 1 and 2 (the generalization for a higher number of escapes is straightforward). By *escape* we mean a route that allows the particle to leave the inner region permanently. The particular escape chosen by a particle is dependent on the initial conditions of that particle. For a given dynamical system and a given energy, the set of points in phase space which correspond to initial conditions such that the particle chooses escape 1 is the *basin* corresponding to escape 1; the basin corresponding to escape 2 is defined analogously. A point in phase space is defined to be a boundary point if every neighborhood of such a point contains points belonging to both basins. The basin boundary is the set formed by all the boundary points.

This system is chaotic if its basin boundary is fractal. Near a fractal basin boundary the points belonging to the different basins are mixed in a very complex way, down to arbitrarily small scales. If we draw a plot of the basins with a finite resolution, and amplify a region containing a fractal boundary, then no matter how much we amplify it, we will always find complex structures of intermixing points of both basins. This implies a strong dependency on the initial conditions near a fractal basin boundary.

If a system has a fractal basin boundary, then it has a fractal set of unstable “eternal” orbits, that never escape in the past and in the future (orbits that have never entered nor will ever leave the inner region), called the *invariant set*. The basin boundary is formed by trajectories belonging to the stable manifold of the invariant set, that is, by trajectories that never escape in the future (“trapped” trajectories); the unstable manifold is formed by orbits that do not escape for $t \rightarrow -\infty$. The invariant set, as well as its stable and unstable manifolds, are sets of zero measure within the phase space. Notice that in general not all the eternal trajectories belong to the invariant set: if the system has a stable periodic orbit for energies above the escape energy, then orbits near this one will also be eternal, and they form a non-zero-measure set of eternal orbits that are not part of the invariant set. These stable orbits have islands of regular behavior surrounding them, where the phase-space flow is integrable and confined to invariant tori.

We note that, for a system (at a given energy) to have a fractal basin boundary, it needs not only to be non-integrable, but also it must be such as to allow the presence of such fractal set of trapped trajectories. In other words, the potential must be such that the particle can bounce back and forth many times before it escapes, if the system is to have a fractal basin boundary.

The presence of a fractal invariant set is the result of transversal crossings of the stable and unstable manifolds of isolated unstable periodic orbits that lie near the openings of the potential, the so-called Lyapunov orbits [2]. The basin boundaries between the different escapes are the stable manifolds of the Lyapunov orbits. The homoclinic and heteroclinic crossings imply a horseshoe symbolic dynamics, which is responsible for the chaos and the fractal character of the basin boundaries. The horseshoe dynamics results also in the existence of a dense set of countable unstable periodic orbits, that must thus exist if the system has a fractal basin boundary.

To give a quantitative measure of the sensibility to initial conditions of a system with a fractal basin boundary, we define the box-counting dimension of the boundary as follows: let two points chosen randomly in a region of the phase space be separated by a small distance ϵ ; it can be shown [1] that the probability that the two points belong to different basins scales as:

$$P(\epsilon) \propto \epsilon^{D-d}, \quad (10)$$

where D is the (integer) dimension of the region where the ensemble of points was chosen; and d is the (possibly non-integer) dimension of the intersection of the region of the basin boundary with this region. If the boundary is non-fractal, then $d = D - 1$, while if the boundary is fractal, we have $d > D - 1$. By choosing randomly a large number of points in a region of the phase space for a certain fixed ϵ , we can calculate $P(\epsilon)$ numerically, and doing this for several values of ϵ , we can calculate the fractal dimension d ; this is the method we use in this article.

If our system has a stable periodic orbit for energies above escape, then as we said above it has a set of positive measure of non-escaping regular orbits confined to tori in phase-space. Escaping orbits that come close to this set stay in its neighborhood for a long time before leaving; in other words this set is “sticky” [12]. This complicates the task of calculating the box-counting dimension, for it demands a greater integration time. We also observe that for this same reason, the boundary between the escaping and the non-escaping regular orbits does not have a well-defined box-counting dimension.

We observe that since both the fractal structure of the basin boundary and its dimension d are topological invariants of the dynamical system, they are valid characterizations of chaos in general relativity.

IV. DYNAMICS OF MATERIAL PARTICLES

In this section, we investigate the movement of material test particles in the metric (9) for some choices of the multipole moments D , Q and O . Important properties of the dynamics can be understood by means of the “effective potential” associated with this metric [9].

Besides the energy and the z component of the angular momentum, there is another quantity which is conserved along the trajectory of a test particle, namely its rest mass. Since we are using units such that the rest mass is unity, the conserved quantity is:

$$g^{\mu\psi} p_\mu p_\psi = E^2 g^{tt} + L_z^2 g^{\phi\phi} + f(\dot{r}^2 + \dot{z}^2) = 1, \quad (11)$$

where $f = -g_{rr} = -g_{zz} = e^{2(\psi-\gamma)}$. The boundary of the region in the configuration space which is accessible to the particle is found by setting $\dot{r} = \dot{z} = 0$:

$$E^2 g^{tt} + L_z^2 g^{\phi\phi} - 1 = 0. \quad (12)$$

The “effective potential” $V(r, z)$ is then given by:

$$V(r, z) \equiv E^2 = \frac{1 - L_z^2 g^{\phi\phi}}{g^{tt}}; \quad (13)$$

Substituting for the Weyl metric (1), we have:

$$V(r, z) = e^{2\psi} \left(1 + \frac{e^{2\psi} L_z^2}{r^2} \right); \quad (14)$$

The region on the rz plane accessible to the particle is given by $V(r, z) \leq E^2$. Using equation (9) for ψ , we thus have an expression for the effective potential in terms of the multipole moments. We note that V depends only on ψ , and not on γ .

The equations of motion for the test particles is:

$$\ddot{x}^\mu + \Gamma_{\alpha\beta}^\mu \dot{x}^\alpha \dot{x}^\beta = 0, \quad (15)$$

and using eqs. (II) and (1) we cast them in the convenient form:

$$\ddot{r} = -\frac{1}{2f} [g_{,r}^{tt} E^2 + g_{,r}^{\phi\phi} L_z^2 + f_{,r} (\dot{r}^2 - \dot{z}^2) + 2f_{,z} \dot{r} \dot{z}]; \quad (16)$$

$$\ddot{z} = -\frac{1}{2f} [g_{,z}^{tt} E^2 + g_{,z}^{\phi\phi} L_z^2 + f_{,z} (\dot{z}^2 - \dot{r}^2) + 2f_{,r} \dot{r} \dot{z}]. \quad (17)$$

The evolution of t and ϕ is given by the quadratures (II).

In the following subsections, we will analyze the dynamics for some interesting choices of D , Q and O . For bounded trajectories, this system was shown through Poincaré sections to be chaotic [10,11].

A. Dipole Potential

If we make $Q = O = 0$ in (9), we have a pure dipole field together with a Schwarzschild black hole. Bounded trajectories of this system have been studied, and chaos has been found using Poincaré sections [11]; the classical equivalent of this system can be shown to be integrable, so the chaos is due to general relativistic contributions to the dynamics. We shall now study this system in the open regime, that is, with energies large enough as to allow them to escape either to infinity or to the event horizon.

In figure 1 we show some contour levels of the effective potential $V(r, z)$ for $D = 3 \times 10^{-4}$ and $Q = O = 0$, with $L_z = 3.0$. The first feature we notice is the “tunnel” formed by the equipotential curves for small values of r , that leads to the event horizon (remember that in these coordinates, the event horizon is given by $r = 0$ and $|z| \leq 1$). This is the route followed by particles that fall into the black hole. We observe that V is invariant under the transformation $z \rightarrow -z$; $D \rightarrow -D$.

If a particle has high enough energy (E^2 higher than about 0.94 for the parameters of fig. 1), it can also escape to infinity. This is shown clearly in fig. 1 by the opening that appears in the equipotentials for high energies.

Now let us pick one specific value for the energy, for instance $E^2 = 0.95$. At this energy, a particle's orbit can have three outcomes: (1) escape into the black hole; (2) escape to infinity; and (3) keep bouncing back and forth forever, and never leave the inner region. The concave shape of the equipotential for this energy suggests that we have stable trapped orbits and thus regions of regular behavior in the phase space. This is indeed the case, as we will see shortly.

To investigate the nature of the basin boundaries, we need a portrait of the basins; to do this, we define a 2-dimensional section of the 3-dimensional energy shell of the phase space that is accessible to the particle. For $E^2 = 0.95$ we define this section as the set of initial conditions with spatial coordinates lying on the segment given by $z = 0$ and $15 \leq r \leq 25$, with velocities given by:

$$\dot{r} = v \cos(\theta); \quad \dot{z} = v \sin(\theta), \quad (18)$$

where

$$v = (\dot{r}^2 + \dot{z}^2)^{1/2} = \frac{1}{f} (1 - E^2 g^{tt} - L_z^2 g^{\phi\phi}) \quad (19)$$

is fixed by the conservation equation (11), and $0 \leq \theta \leq 2\pi$. This section is thus a topological segment of a cylinder embedded within the phase space, and we will denote it by S .

To obtain numerically the intersection of the basins with this section, we divide the intervals $15 \leq r \leq 25$ and $0 \leq \theta \leq 2\pi$ into 400 equal parts each; this defines a grid on S composed of 400×400 points. For each of these points, we integrate numerically the equations of motion for the dipole metric, and record the outcome: if the trajectory falls into the black hole (numerically, if r becomes too small, or less than 0.5 in this case), that initial condition belongs to basin 1; if the trajectory escapes to infinity (numerically, if r or z becomes too large, larger than 60 in this case), it belongs to basin 2; and if after a certain proper time τ_{max} (in this case $\tau_{max} = 10000$) the trajectory chooses none of the two escapes above, then we admit that it belongs to the set of “trapped” trajectories that never leaves the confining region. We choose τ_{max} such that the set of “trapped” trajectories is well resolved for the scale of the grid we use.

The results of this calculation are shown in fig. 2a. A black dot means that the corresponding point (r, θ) in S belongs to basin 1; a white dot indicates that it belongs to basin 2; and a grey dot means it belongs to the set of “trapped” trajectories. We notice a complex Cantor-like mixing of basins, indicating that the structure continues down to smaller scales. This is confirmed by the amplification of a detail of figure 2a, shown in fig. 2b. The area covered by fig. 2b is about 10 orders of magnitude smaller than that of fig. 2a, giving strong evidence that the basin boundary is indeed fractal. We note that the set of trapped trajectories has as we suspected a non-zero measure; this is clear from fig. 2a. As we discussed in section III, we expect them to form a regular island in phase space. The intersection of these orbits with a Poincaré section should define closed curves. This can in fact be observed in fig. 3a, which shows the intersection of some of these trapped orbits with the surface of section $z = 0$. The parameters are the same as in fig. 2. The regular island shown in fig. 3a appears to be the only one present in the system for these parameters.

To have a more precise and quantitative characterization of the fractal structure seen in fig. 2, we proceed to the calculation of the fractal dimension, as discussed in section III. The random points are chosen in S , and for each point (r, θ) we find through numerical integration to which of the basins it belongs, and then do the same for two nearby phase space points given by $r + \epsilon$ and $r - \epsilon$ and the same θ . If all three points do not belong to the same basin, then the point (r, θ) is considered an “uncertain” point, meaning that it lies close to a basin boundary. For a large number N of points randomly chosen in S , the fraction of uncertain points is $f(\epsilon) = N'/N$, where N' is the number of uncertain points found in the sample of N points. For N large enough, f is proportional to P in eq. (10); finding in this way f for several values of ϵ , a log-log plot of $f(\epsilon)$ should give a straight line, and the basin boundary dimension d is found by the angular coefficient through eq. (10). For reasons explained in sec. III, we calculate d choosing points in a region that does not intersect the trapped regular region. By getting rid in this way of the “stickiness” of the regular region, we are able to obtain a meaningful result for d .

The results are shown in fig. 3b. We have chosen N such that $N' > 100$; this means a statistical uncertainty of 10% in f . We see that the points lie on a clearly defined straight line; the angular coefficient is $\alpha = 0.47 \pm 0.02$, which gives a dimension of $d = 1.53 \pm 0.02$, showing unambiguously that the boundary is fractal. We remember that d is the dimension of the intersection of the basin boundary with the 2-dimensional section S ; the dimension of the basin boundary in the accessible 3-dimensional space is $d + 1$, and its dimension in the full 4-dimensional phase-space is $d + 2$. We have calculated d for some subregions of S , and we have obtained always the same value to within the statistical uncertainty, showing that the method is self-consistent and the result is meaningful.

We have studied how the box-counting dimension varies as we change the various parameters of the metric. If $D = 0$, a particle needs an energy E higher than 1 to be able to escape to infinity. If $D \neq 0$, the escape energy becomes less than 1, and depends on the angular momentum L_z . We denote the escape energy by $E_0 = E_0(L_z)$. The basin boundary dimension d is defined only for $E > E_0$. We have found that for $E > 1$, $d = 1$ (to within the statistical error), and the motion is regular. We have verified this result for several values of L_z and E , and three different values of D ; this feature is also suggested by the forms of the equipotentials for $E > 1$.

We have also investigated how d varies with the dipole strength D . In the limit $|D| \rightarrow \infty$, we have a field dominated by the dipole component; the geodesics defined by a pure dipole field are integrable, and thus we expect d to approach 1 for high values of D . If we decrease D enough, we end up reaching a value D_0 below which the particle can no longer escape to infinity, and d is no longer well defined. Near $D = D_0$, with $D > D_0$, the opening of the equipotential to the escape to infinity is small, and the particle is likely to bounce more times before it escapes through this route than in the case of higher values of D , and we accordingly expect the chaos to be “larger” in this case, that is, d to be larger. These features are indeed verified in a plotting of d versus D for $E^2 = 0.95$ and $L_z = 3.0$, shown in fig. 4. For these values of D and L_z , we have $D_0 \equiv 2.5 \times 10^{-4}$. The system is regular ($d = 1$) for $D \geq 9 \times 10^{-4}$, d reaches its highest value of about 1.6 at $D = D_0$.

B. Quadrupole Potential

We next turn to the case $D = O = 0$. This quadrupole field has a reflection symmetry with respect to the z axis: the metric is unchanged by $z \rightarrow -z$. For $Q > 0$, the open equipotentials are similar to the pure dipole case discussed above (except for the aforementioned symmetry). A more interesting choice is $Q < 0$; in this case, as shown in fig. 5, there are two different escapes to infinity, besides the escape into the event horizon. In this case, we can choose an energy level such that the set of trapped trajectories has zero measure, and therefore there are no regular regions in phase space, as in the dipole case. As stated in section III, this is desirable numerically, since the presence of trapped trajectories increases very much the integration times needed. The energy we have chosen is $E^2 = 0.97$, with $L_z = 2.6$.

We proceed as we did for the dipole case. We choose initial conditions in the segment $r = 25.0$, $|z| < 25.0$; the velocities are given by (18). The results are in fig. 6a, with black dots denoting trajectories that escape upwards, white dots denoting trajectories that escape backwards, and grey dots denoting trajectories that fall into the event horizon. Figure 6b shows an amplification of a very small area of fig. 6a, and the absence of smoothness in the basin boundary shows clearly its fractal character. The fractal dimension was computed as described above, and the value we obtained was $d = 1.60 \pm 0.03$. We have calculated d for other values of the energy and angular momentum, and we found that, as opposed to the dipolar halo system studied in the previous section, this system is chaotic for $E > 1$. In fact, we found that the boundary is fractal for arbitrarily large values of the energy (for $Q < 0$), as far as we have been able to investigate; this is an important difference between the dipolar and quadrupolar halos.

Since the basin boundary between the escapes is the stable manifold of an invariant set, we have associated with the chaos in the choice of the escape route a chaos in the escape time as well, as is well-known in chaotic scattering. This happens because orbits starting from very close initial conditions may make a different number of bounces before escaping, leading to very different escape (proper) times. We have illustrated this by finding numerically the escape proper times τ_e for orbits starting from a fixed position $r = 25$, $z = 0$, for several velocity angles θ , as defined by eq. (18). We plot $\tau_e(\theta)$ in fig. 7a. The “spiked” character of the graph is striking, suggesting a fractal structure. This is confirmed by fig. 7b, which shows that the function $\tau_e(\theta)$ has a fractal set of singular points, where $\tau_e(\theta)$ goes to infinity; this set is the intersection of the line of initial conditions with the basin boundary. We observe that the escape time τ_e is to some extent arbitrary, because it depends on where we stop the integrations of the trajectories before we consider them to have escaped. However, the fractal structure seen in fig. 7 is topological, and is not affected by this choice.

In order to gain more insight into the fractal structure of the basin boundary and its related complex dynamics, we now define a surface of section in phase space denoted by \mathcal{P} and given by $\dot{z} = 0$, for a given E and L_z . We define I_n ($n \geq 1$) as the set of points on the surface of initial conditions S that generate orbits that cross \mathcal{P} at least n times in the negative direction (that is, satisfying $\dot{z} < 0$) before escaping. Obviously I_n is a subset of I_k if $k < n$, and we have that:

$$I_1 \supset I_2 \supset I_3 \supset \dots \quad (20)$$

For systems without regular trapped orbits (such is the case of the quadrupole field with the parameters of fig. 7), the basin boundary is given by $\lim_{n \rightarrow +\infty} I_n$. If we let I_n , with n being a negative integer, denote the set of points in S corresponding to past-directed orbits which cross \mathcal{P} in the negative direction at least $|n|$ times, then the unstable

manifold of the repeller set is analogously given by $\lim_{n \rightarrow -\infty} I_n$. Defining now the set $R_n = I_n \cap I_{-n}$, the repeller set is given by $\lim_{n \rightarrow +\infty} R_n$. This simply states that the repeller set is the intersection of its stable and unstable manifolds.

The mechanism of the construction of the fractal basin boundary by the dynamics of the system may be followed by examining the sets I_n ($n > 0$). Figs. 8a, 8b and 8c show I_1 , I_2 and I_3 respectively, using the same grid as that of fig. 7a. As n increases, the structure of I_n becomes more and more complicated: every step $I_n \rightarrow I_{n+1}$ results in taking from I_n increasing numbers of ever thinner strips, intercalatedly. We recognize this as the mechanism for the construction of a Cantor set, in the limit $n \rightarrow +\infty$.

We can follow in the same way the construction of the invariant set itself: in fig. 8d we show R_2 ; compare this with fig. 8b.

The Newtonian system equivalent to the multipole field we are dealing with is given by the Hamiltonian:

$$H = \frac{1}{2} (p_r^2 + p_z^2) + V(r, z), \quad (21)$$

where $V(r, z)$ is the effective potential:

$$V(r, z) = \frac{L_z^2}{2r^2} - \frac{1}{r} + \psi(r, z), \quad (22)$$

and ψ is given by (9). For the dipole field ($Q = O = 0$), as we mentioned before, the Hamiltonian (21) is integrable. For the quadrupole field, however, it is not [10], so we expect to have a fractal basin boundary for this case as well. Figure 9 shows some level contours of V with $L_z = 2.6$ and $Q = -4 \times 10^{-6}$, $D = O = 0$; these are the same parameters we have used for the relativistic case. For this negative value of Q , we have two escapes (for $Q > 0$, there is only one escape). Since we want to compare the Newtonian and the relativistic cases, we choose the energy to be $E - 1$, where E is the energy we used in the relativistic case, which gives -0.0151 . We proceed as in the relativistic case to calculate the basin boundary dimension. The initial conditions are chosen in the segment $|z| < 5$, $r = 13$. The result is $d = 1.64 \pm 0.02$, which is roughly the same (actually a little larger) value we obtained for the relativistic case.

C. Quadrupole + Octopole Potential

The last case we investigate in this section is the field formed by the superposition of the quadrupole and octopole components, $D = 0$ with $Q, O \neq 0$. The octopole term breaks the reflection symmetry of the quadrupole potential, as can be seen in fig. 10, which shows some level contours of the effective potential for $D = 0$, $Q = -4 \times 10^{-6}$, $O = -1 \times 10^{-7}$ and $L_z = 2.6$. We still have three escapes as in the previous case, but the equipotentials are distorted, and are no longer symmetrical with respect to the $z = 0$ axis. We select the energy $E^2 = 0.97$, and pick the initial conditions on the segment $|z| < 20$, $r = 20$. Using these parameters, we have calculated the basin boundary dimension, and found $d = 1.59 \pm 0.02$, which is practically the same value obtained for the pure quadrupole field $O = 0$. If we calculate d for the pure octopole field $O = -10^{-7}$, $Q = 0$, keeping the other parameters fixed, we find $d = 1.70 \pm 0.02$, which is *larger* than the value obtained for the mixed field. This is a somewhat surprising result, and it shows that a “more complicated” field does not necessarily result in a more complicated (or “more chaotic”) motion.

V. THE NULL GEODESICS

We will now study the dynamics of the null geodesics in the metric (9). For null geodesics, $ds^2 = 0$, and we have:

$$E^2 g^{tt} + L_z^2 g^{\phi\phi} + f(\dot{r}^2 + \dot{z}^2) = 0, \quad (23)$$

with $f = -g_{zz} = -g_{rr}$. The effective potential is then given by:

$$\frac{E^2}{L_z^2} \equiv \frac{1}{b^2} = V(r, z) = -\frac{g^{\phi\phi}}{g^{tt}} = \frac{e^{4\psi}}{r^2}, \quad (24)$$

where b is the impact parameter with respect to the z axis. The curve $V(r, z) = 1/b^2 = \text{const}$ is the boundary of the accessible regions of the rz plane to a particle having an impact parameter of b . We notice that in the case of massive particles, the effective potential depends separately on E and L_z , while for the case of massless particles, it

only depends on the ratio $E/L_z = b$. The equation of motion for the null geodesics is eq. (IV) and (II), with E and L_z related by $b = L_z/E$.

In the case of the dipole field ($Q = O = 0$), we find that below a certain value of the impact parameter b the equipotential curves open, and the orbits can either fall into the event horizon or escape to infinity. We find, however, by numerical calculations of pictures of the basins, which show regular basin boundaries, and by the computation of the basin boundary dimension, which gives $d = 1$ to within the statistical uncertainty, that the basin boundaries are regular and the system presents no chaos. This result holds for all values of D and b we have investigated, and it seems safe to conclude that massless test particles in the field of a black hole surrounded by a dipolar material halo move in regular orbits.

When we introduce terms of higher order in the multipolar expansion of the halo, this situation changes. We illustrate this with a pure quadrupolar halo. If $Q > 0$, there are only two escapes (towards infinity and towards the event horizon), and the orbits are again regular. If $Q < 0$, however, we have three escape routes (towards the event horizon, towards $z \rightarrow \infty$ and towards $z \rightarrow -\infty$), and chaotic behavior arises. This can be seen in fig. 11, where we show some equipotential curves for $Q = -0.05$, with $D = O = 0$. Choosing $b^2 = 12.5$, we obtain a picture of the basins by numerical integration, with the initial conditions in the segment $r = 2$, $|z| < 2$. The result is shown in fig. 12a, and an amplification of several orders of magnitude shows (fig. 12b) that the basin boundary is fractal. This is further confirmed by the calculation of the basin boundary box-counting dimension, which yields $d = 1.25 \pm 0.02$. We have verified that an octopole halo also gives rise to chaos, as must be the case for multipole terms of higher order.

Now we make some general remarks on the motion of massless particles in the metric (9). The absence of stable periodic orbits, and therefore of a non-zero measure set of confined orbits, was verified in all cases we have investigated, leading us to believe that this is a general feature of the motion of zero mass particles in the black-hole-halo field; we speculate that this may be the case in all metrics. We also observed that in all cases in which there are only two escapes (as for instance in the dipolar halo field and in the quadrupolar field with $Q > 0$), the motion of zero rest mass particles is always regular, as opposed to the motion of material particles in the same fields. When there are three or more escapes, on the other hand, chaotic behavior appears. We have found, however, that the motion of massless particles is always less chaotic than the motion of massive particles for the same field, for all cases investigated by us.

VI. CONCLUSIONS

We have studied the escape dynamics of a general-relativistic system consisting of a non-rotating black hole surrounded by a multipolar halo, which can be thought of as the model of the interior of an elliptic galaxy with a central massive black hole. For the case of massive particles, chaos was found in the form of fractal basin boundaries. We single out the case of a dipolar halo, which has a Newtonian counterpart that is known to be integrable; the chaos for this case is thus a result of relativistic corrections to the dynamics. This is compatible with earlier results obtained with bounded orbits [10]. Also for this case, we have investigated the set of trapped orbits with non-zero measure, and we showed that it is formed by regular orbits, bound to tori in phase space. We have found that this system is not chaotic for energies above 1, which is the escape energy for an isolated non-rotating black-hole. The system appears to be most chaotic (its boundary dimension attains its highest value) for energies near escape.

If the halo is composed by a pure quadrupole term, the situation changes: there can be three escape routes, as opposed to only two present in the dipole case (this happens if $Q < 0$), and in this case the system is chaotic for arbitrarily large values of the energy, as far as we could determine.

In the case of massless particles (null geodesics), we find that the black hole + dipolar halo system is not chaotic, the basin boundary between the escapes being regular for all values of the parameters we have investigated. If we add a quadrupole term to the halo, the motion becomes chaotic if $Q < 0$; the orbits are still regular for $Q > 0$. Terms of higher order also introduce chaos in the system. Contrary to the case of material particles, we have not found any stable periodic orbit, with its accompanying non-zero measure set of confined orbits. We believe the absence of stable periodic orbits of massless particles is a general feature of axisymmetric static gravitational fields.

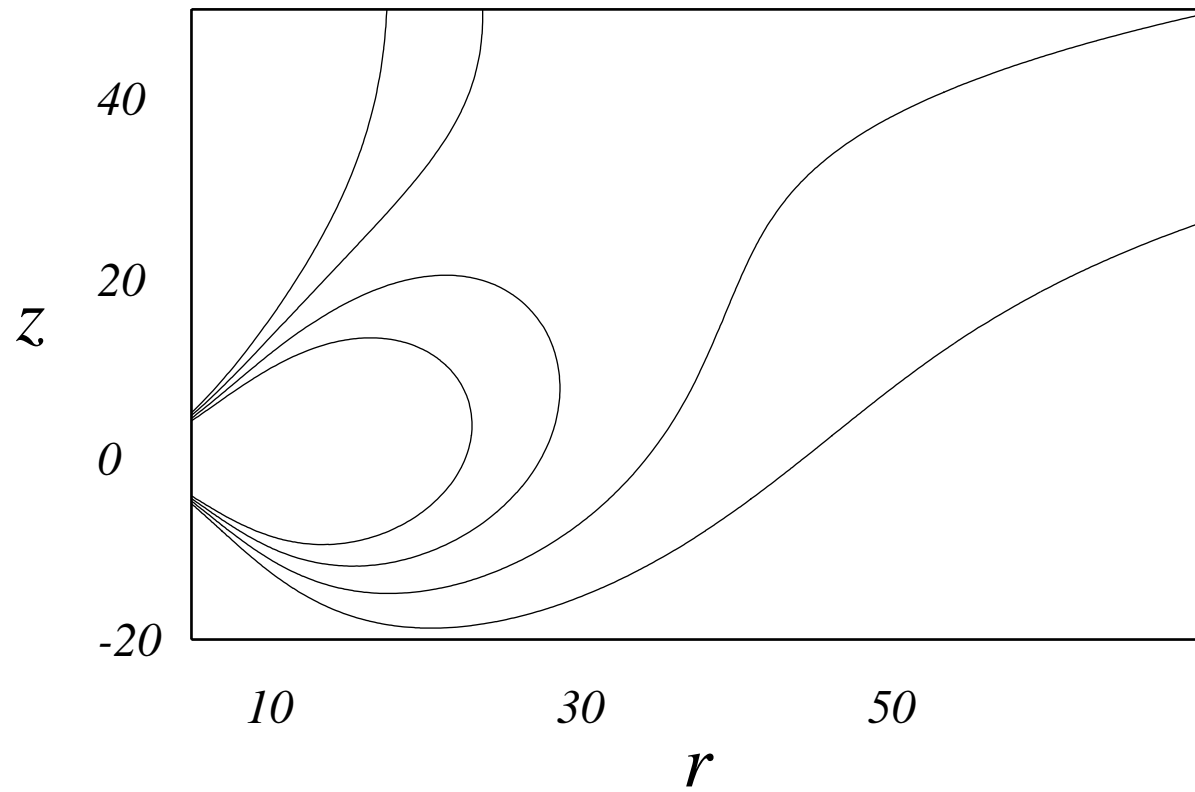
ACKNOWLEDGMENTS

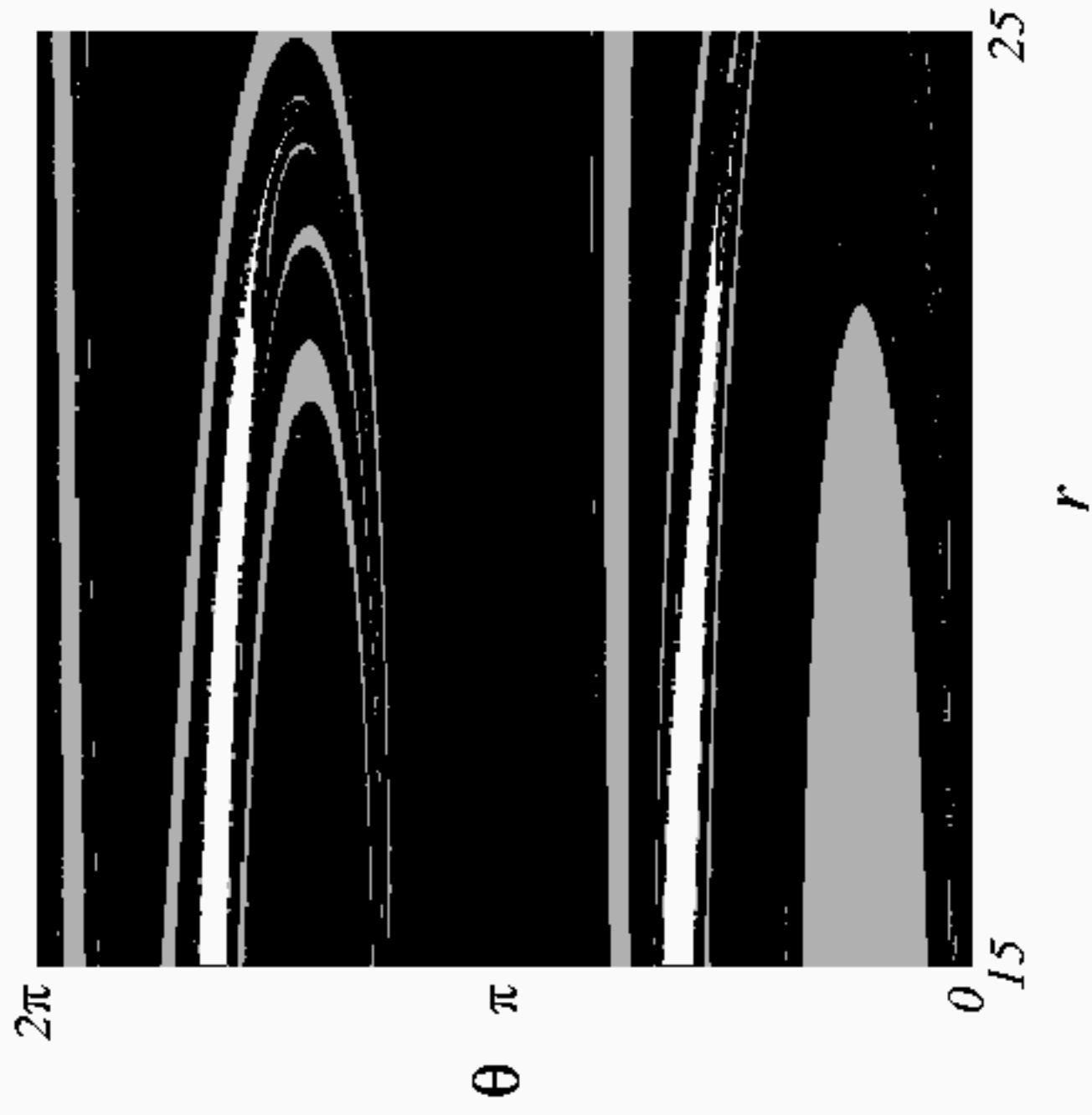
This research was partially funded by FAPESP and CNPq, and we heartily thank them.

- [1] E. Ott, *Chaos in Dynamical Systems*, Cambridge University Press, Cambridge (1993)
- [2] G. Contopoulos, *Astron. Astrophys.* **231**, 41 (1990)
- [3] J. M. T. Thompson, *Proc. R. Soc. Lond. A* **421**, 195 (1988)
- [4] H. B. Stewart, J. M. T. Thompson, Y. Ueda, A. N. Lansbury, *Physica D* **85**, 259 (1995)
- [5] F. Christiansen, P. Grassberger, *Phys. Lett. A* **181**, 47 (1993)
- [6] N. J. Cornish and J. J. Levin, *Phys. Rev. D* **53**, 3022 (1996)
- [7] D. Kramer, H. Stephani and E. Herlt, *Exact Solutions of Einstein's Field Equations*, Cambridge University Press, Cambridge, 1980
- [8] A. G. Webster, *Partial Differential Equations of Mathematical Physics*, Dover Publications, New York (1966)
- [9] C. W. Misner, K. S. Thorne, J. A. Wheeler, *Gravitation*, W. H. Freeman and Company, New York (1973)
- [10] W. M. Vieira and P. S. Letelier, *Phys. Rev. Lett.* **76**, 1409 (1996)
- [11] W. M. Vieira and P. S. Letelier, *Phys. Lett. A* **228**, 22 (1997)
- [12] F. Christiansen, P. Grassberger, *Phys. Lett. A* **181**, 47 (1993)

FIGURE CAPTIONS

- Figure 1** Level contours of the effective potential for the dipole field ($Q = O = 0$), with $D = 3 \times 10^{-4}$ and $L_z = 3.0$. The values of E^2 for the equipotentials are, from the inside out, 0.93, 0.94, 0.95 and 0.96.
- Figure 2** Basin portrait of the section S of the phase space (see text) for the dipole field, for $D = 3 \times 10^{-4}$, $L_z = 3.0$ and $E^2 = 0.95$. The black areas correspond to regions of S whose trajectories fall into the event horizon; white areas correspond to trajectories that escape to infinity; and white areas correspond to trajectories that remain trapped inside the confining region. This figure was calculated on a grid of 400×400 points. (b) is a magnification of (a).
- Figure 3** (a) Poincaré section of trapped orbits, with the surface of section $z = 0$, for $D = 3 \times 10^{-4}$, $L_z = 3.0$ and $E^2 = 0.95$. (b) Plot of the fraction of “uncertain” points $f(\epsilon)$ as a function of the separation ϵ (see section 3).
- Figure 4** Box-counting dimension of the basin boundary as a function of the dipole strength D , for $E = 0.95$ and $L_z = 3.0$.
- Figure 5** Level contours of the effective potential for a quadrupole field ($D = O = 0$) with negative Q ($Q = -4 \times 10^{-6}$) and $L_z = 2.6$. The values of E^2 for the equipotentials are, from the inside out, 0.93, 0.94, 0.95 and 0.96.
- Figure 6** Basin portrait for the quadrupole field, with $Q = -4 \times 10^{-6}$ and $L_z = 2.6$. Black areas denote regions whose trajectories fall into the event horizon; gray areas correspond to trajectories that escape towards $z \rightarrow +\infty$; and white areas correspond to trajectories that escape towards $z \rightarrow -\infty$. (b) is a magnification of (a).
- Figure 7** Time of escape versus the velocity angle ($Q = -4 \times 10^{-6}$, $L_z = 2.6$), for $r = 25$ and $z = 0$. (b) is a magnification of (a).
- Figure 8** (a) I_1 , (b) I_2 , (c) I_3 , (d) R_2 , for $Q = -4 \times 10^{-6}$, $L_z = 2.6$ and $D = O = 0$.
- Figure 9** Level contours of the effective potential for the classical quadrupole field with $Q = -4 \times 10^{-6}$ and $L_z = 2.6$. The values of E^2 for the equipotentials are, from the inside out, 0, -0.01, -0.02 and -0.03.
- Figure 10** Level contours of the effective potential for the field with $D = 0$, $Q = -4 \times 10^{-6}$, $O = -10^{-7}$ and $L_z = 2.6$. The values of E^2 for the equipotentials are, from the inside out, 0.94, 0.95, 0.96 and 0.97.
- Figure 11** Level contours of the effective potential for null geodesics for the quadrupole field $Q = -0.05$, $D = O = 0$. The values of b^2 (b is the impact parameter with respect to the symmetry axis) are, from the inside out, 10.0, 15.0 and 20.0.
- Figure 12** Basin portrait for null geodesics with $Q = -0.05$, $D = O = 0$ and $b^2 = 12.5$. Areas in black correspond to trajectories that fall into the event horizon; areas in gray correspond to trajectories that escape towards $z \rightarrow +\infty$, and areas in white denote trajectories that escape to $z \rightarrow -\infty$.



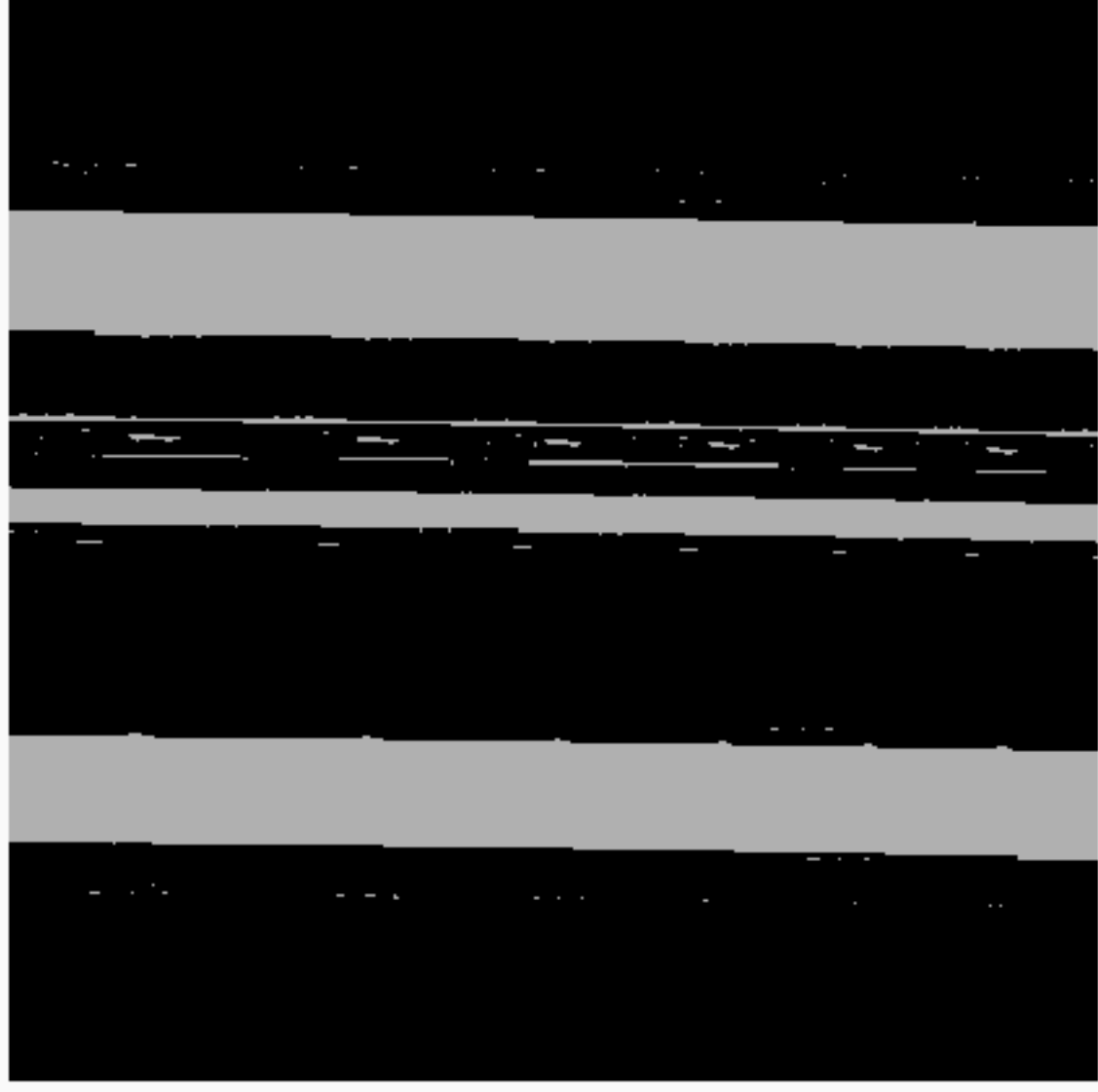


0.7428

θ

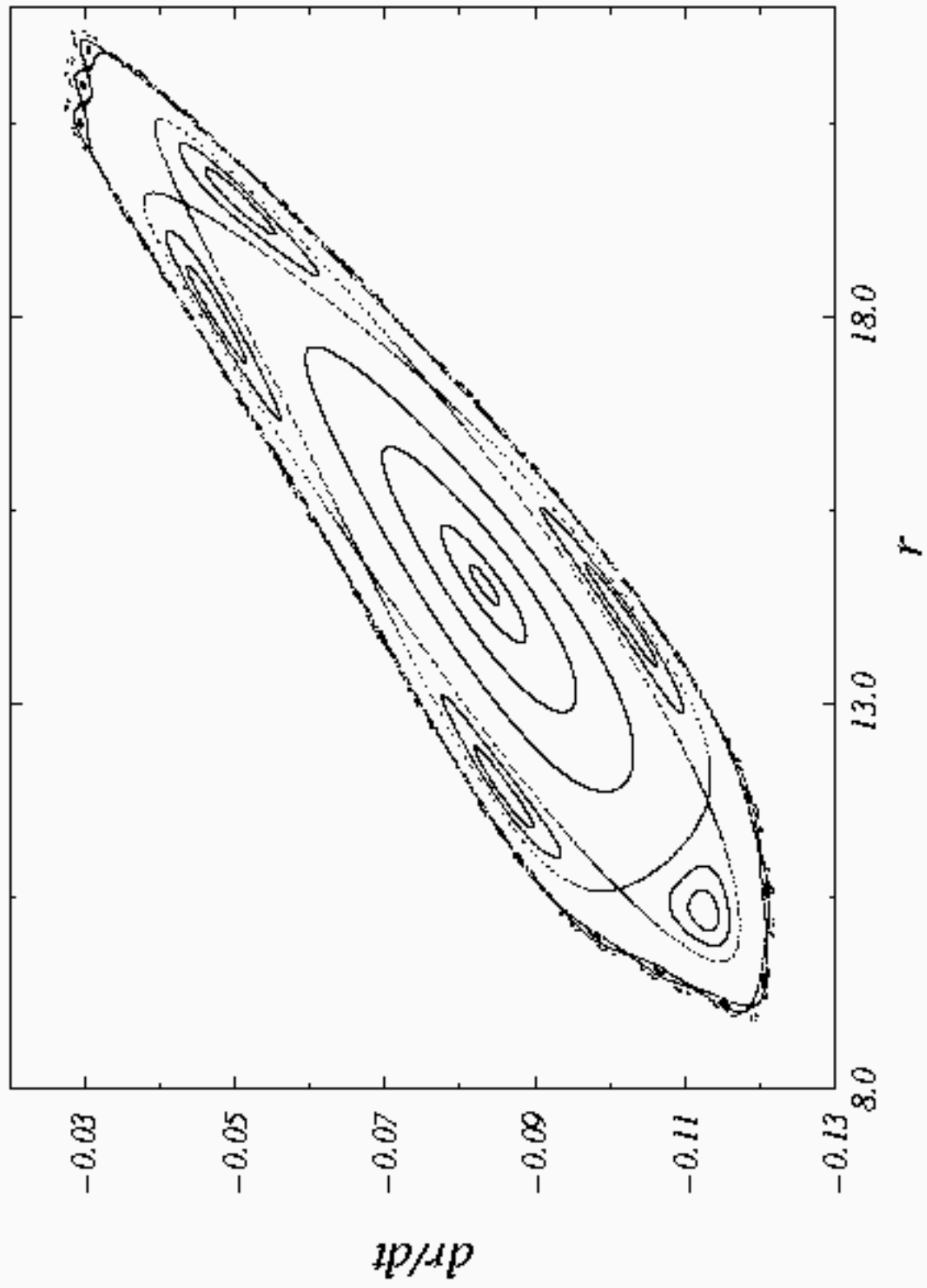
0.7420

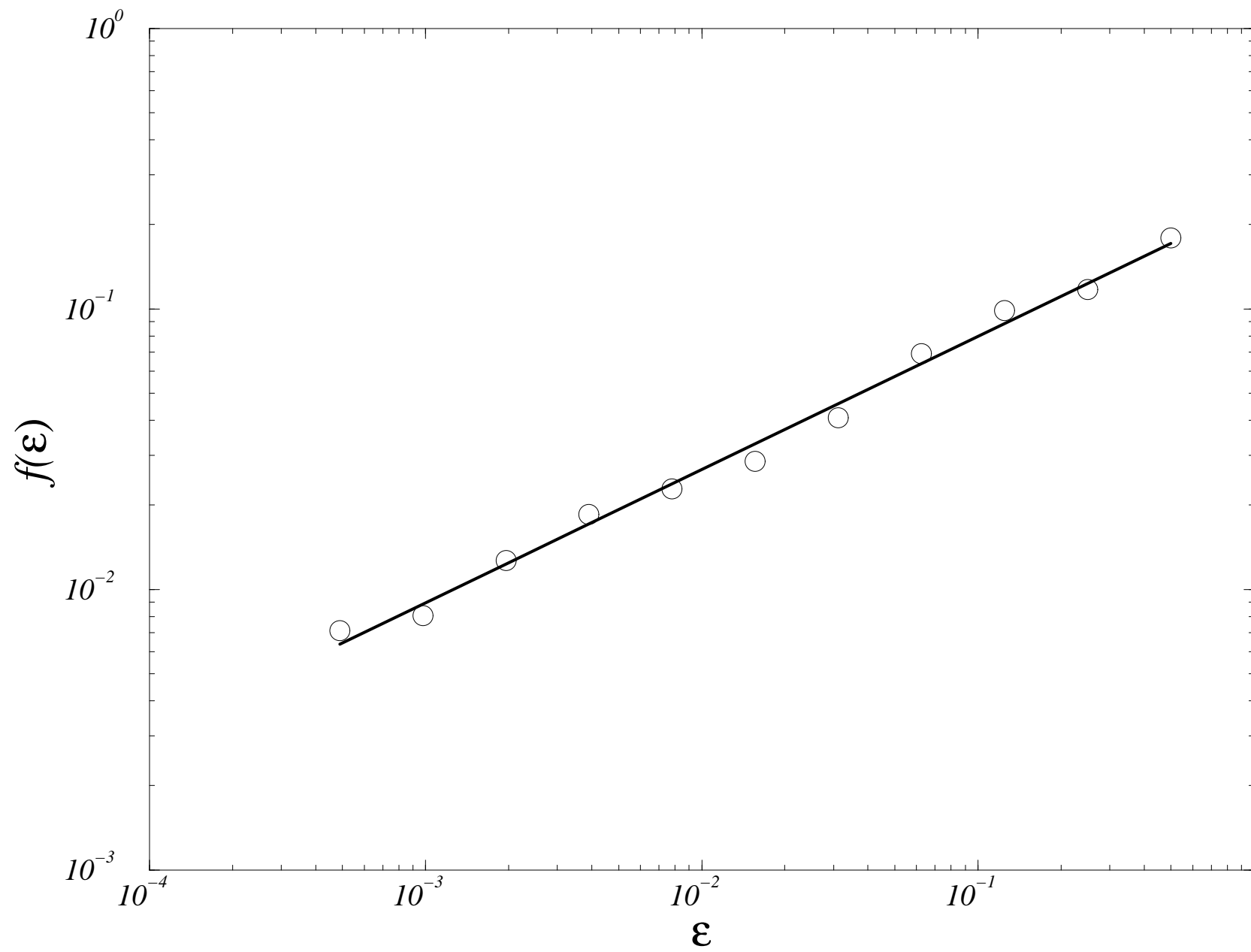
22.324

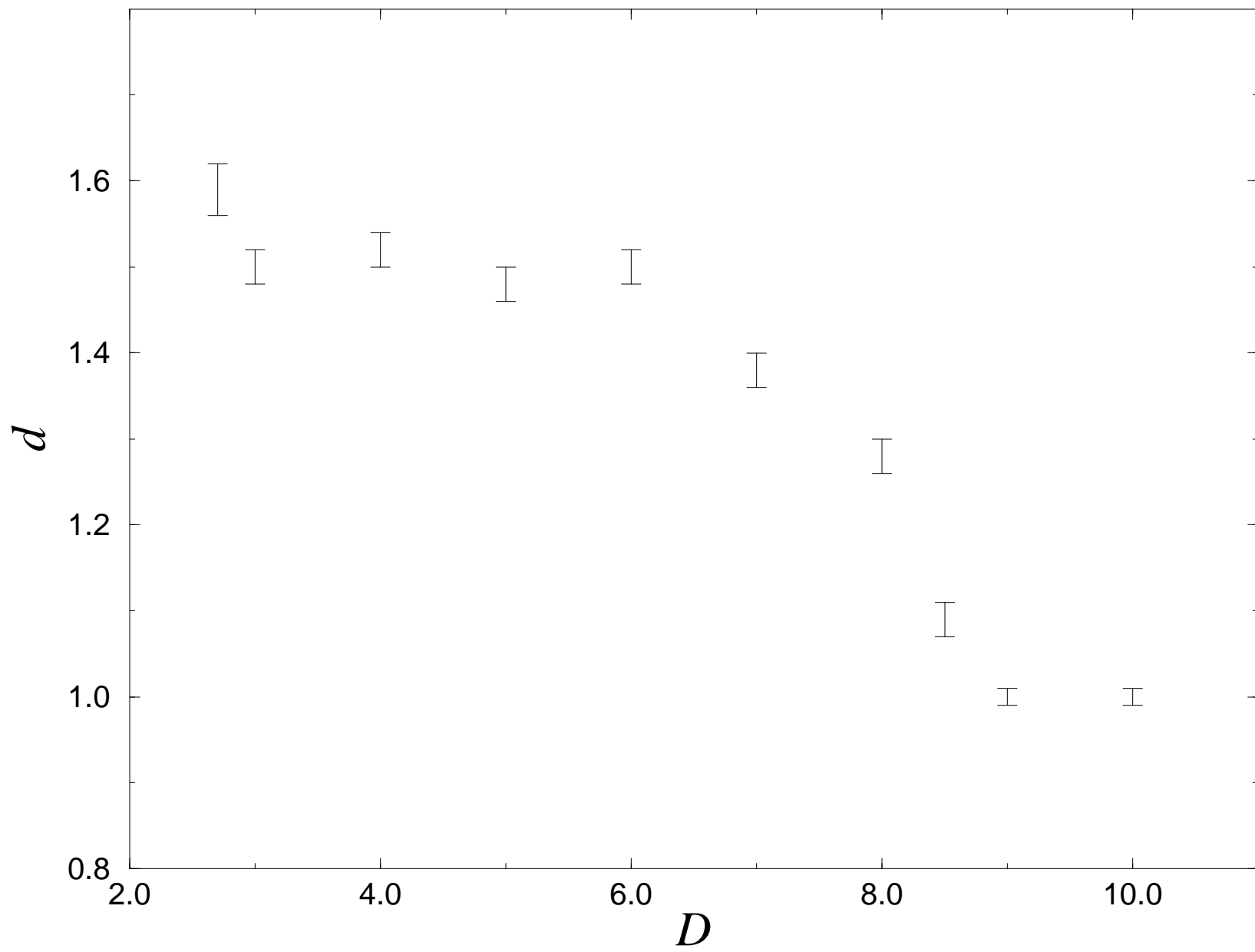


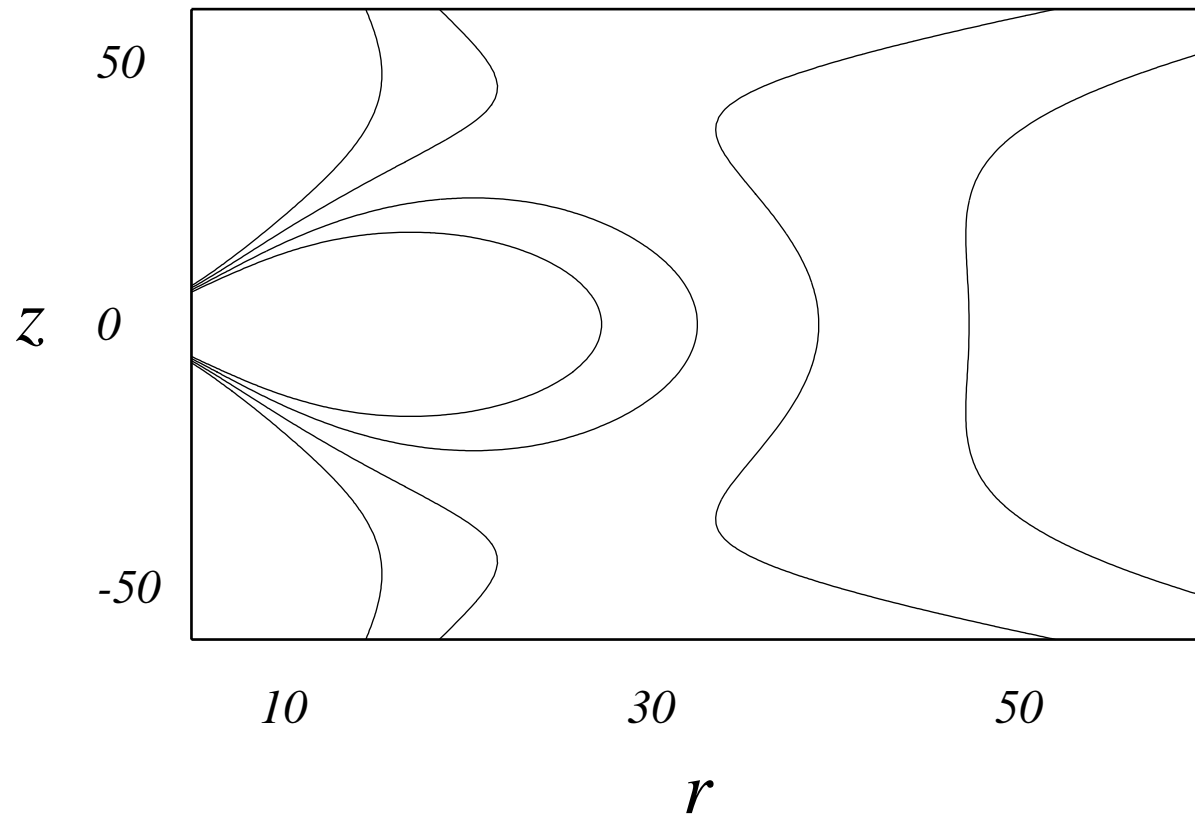
22.324

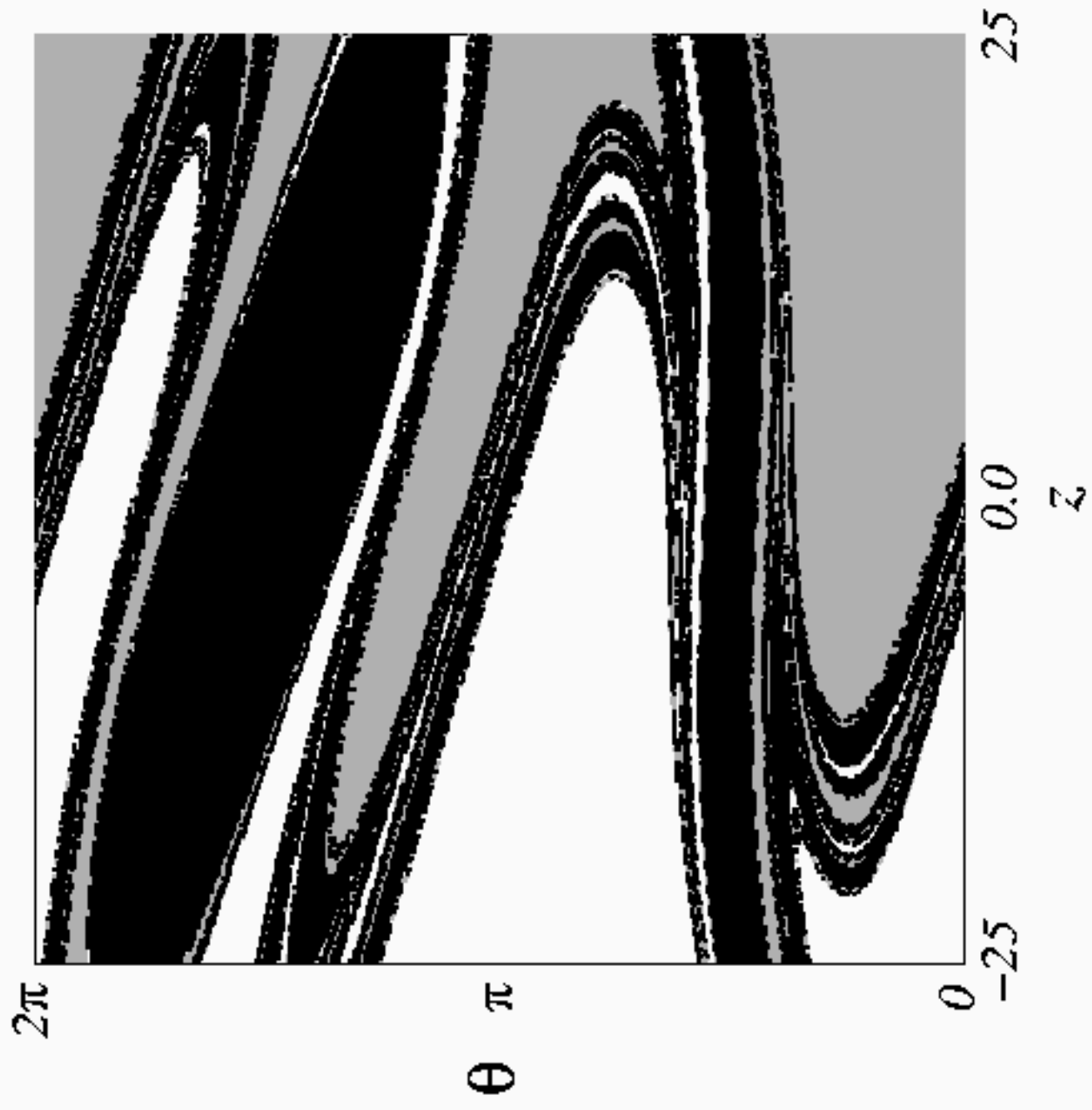
r











0.7624

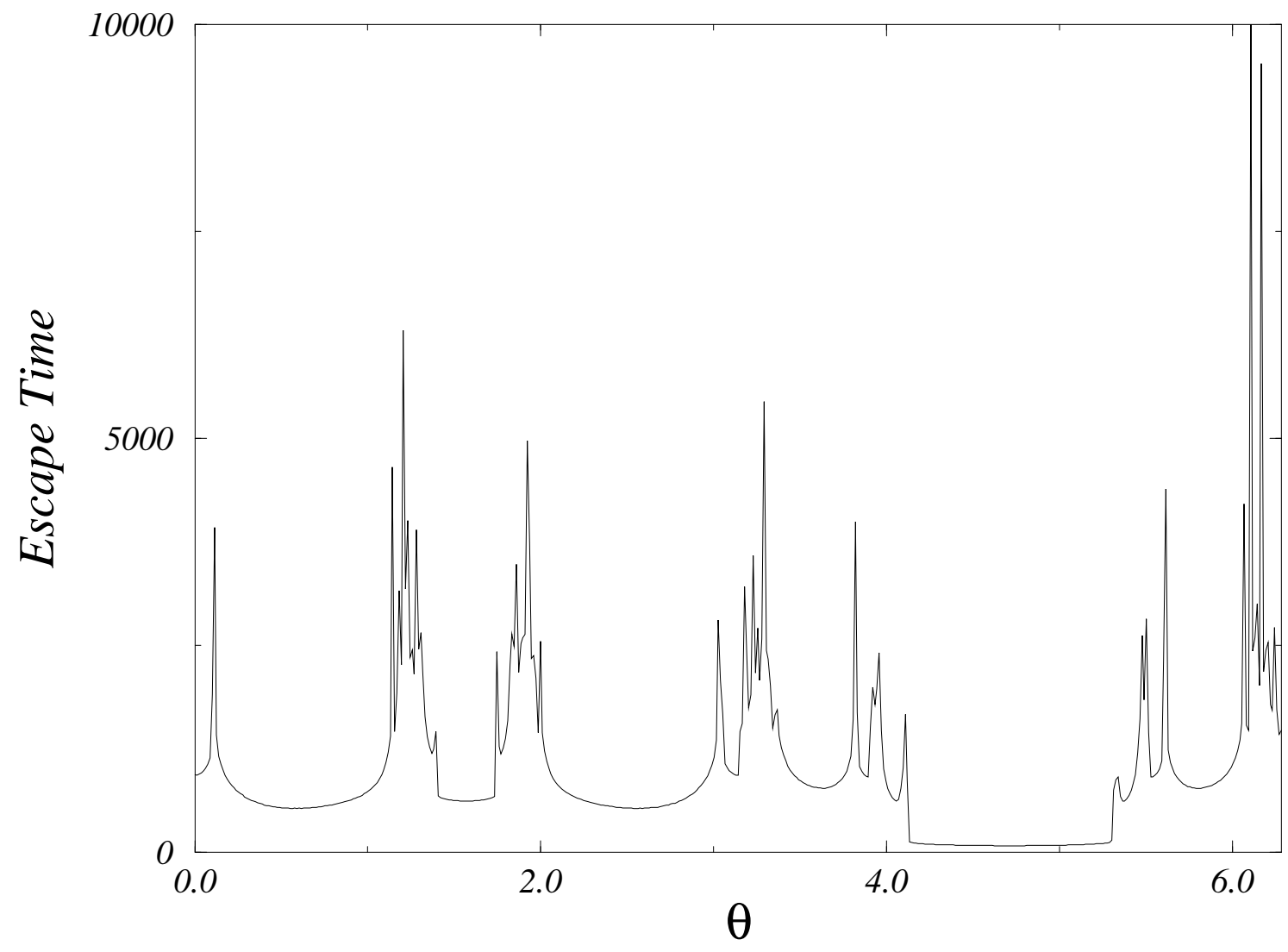
θ

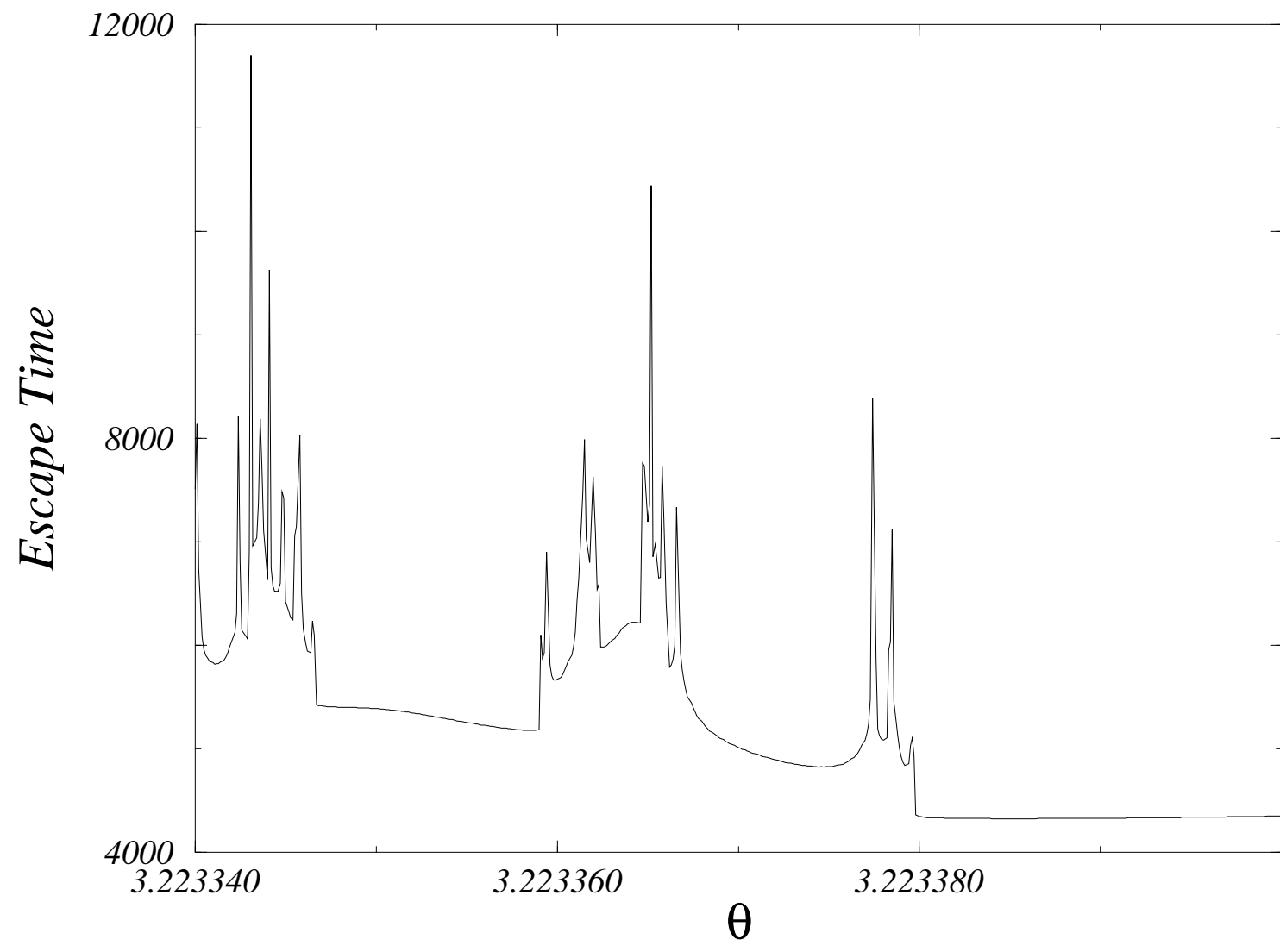
0.7618
-18.633

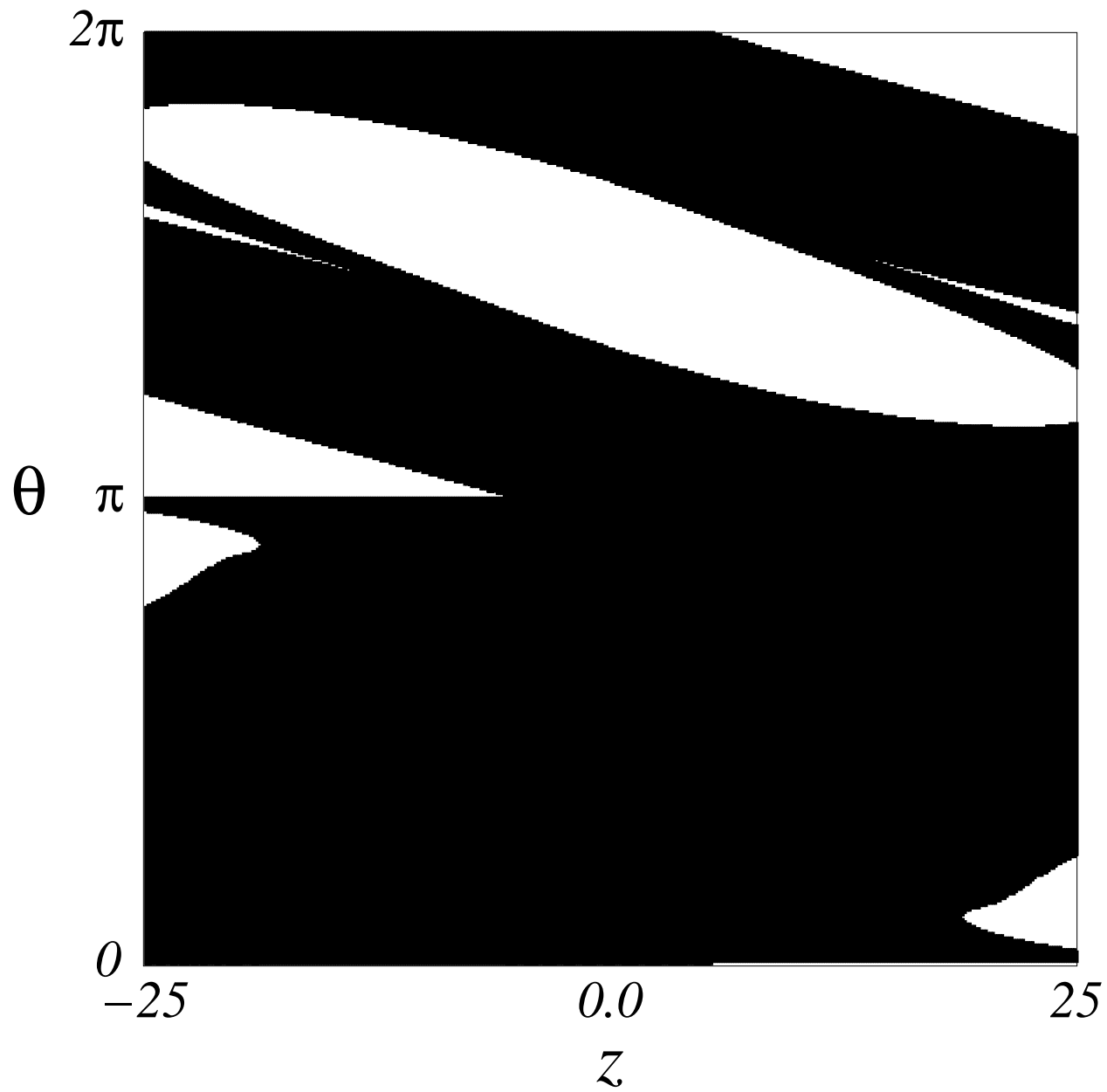
-18.623

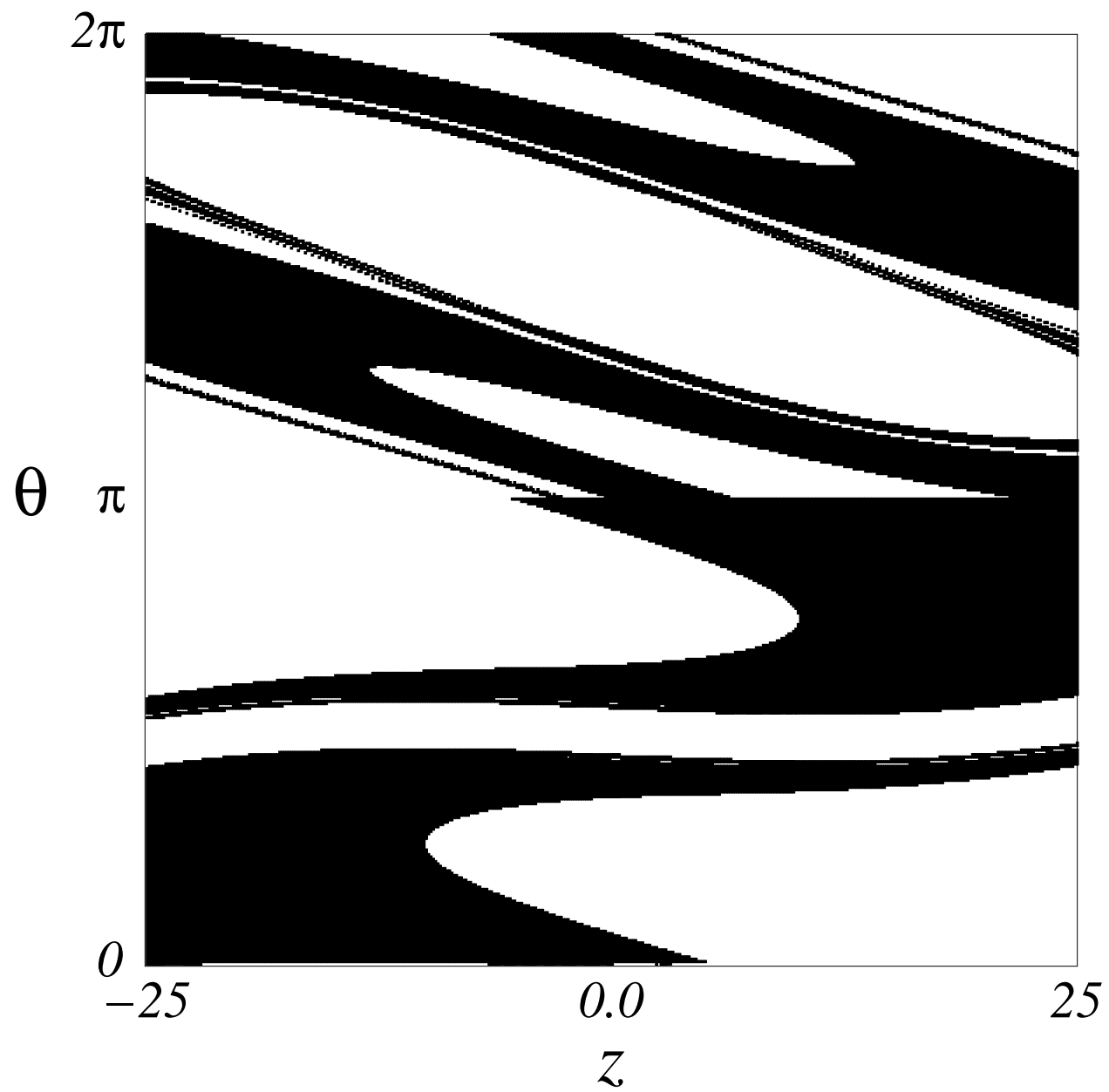
z

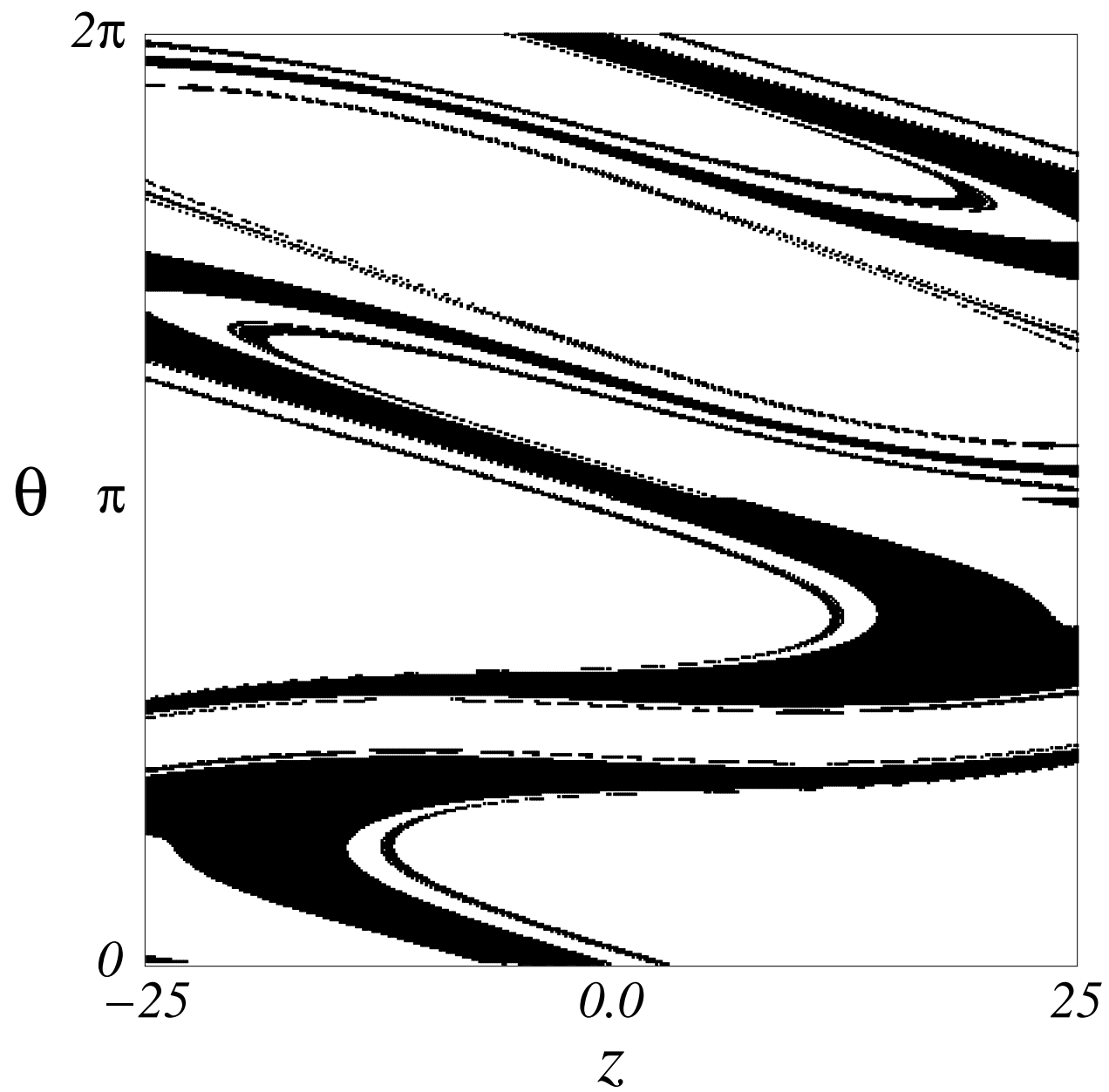


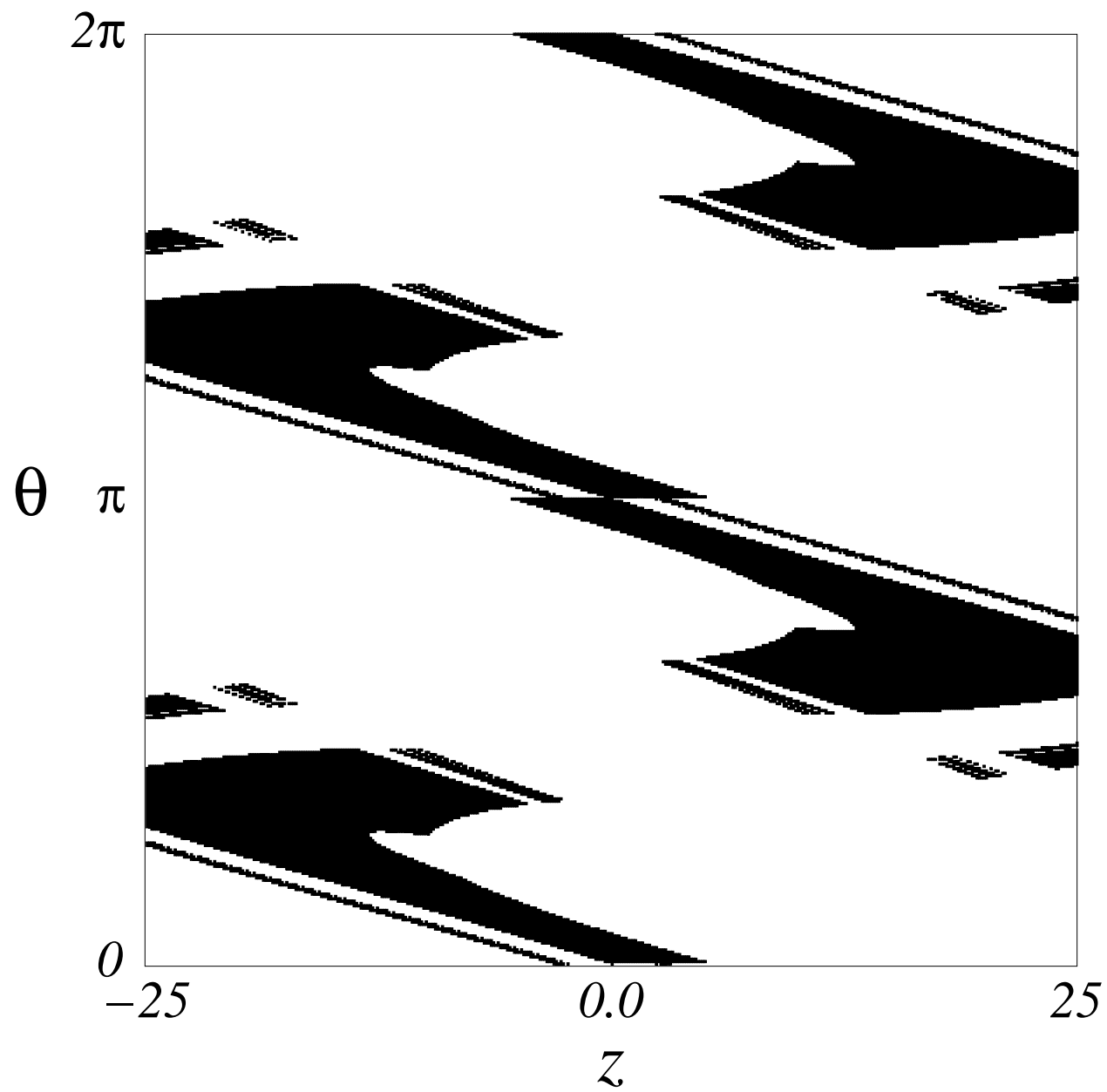


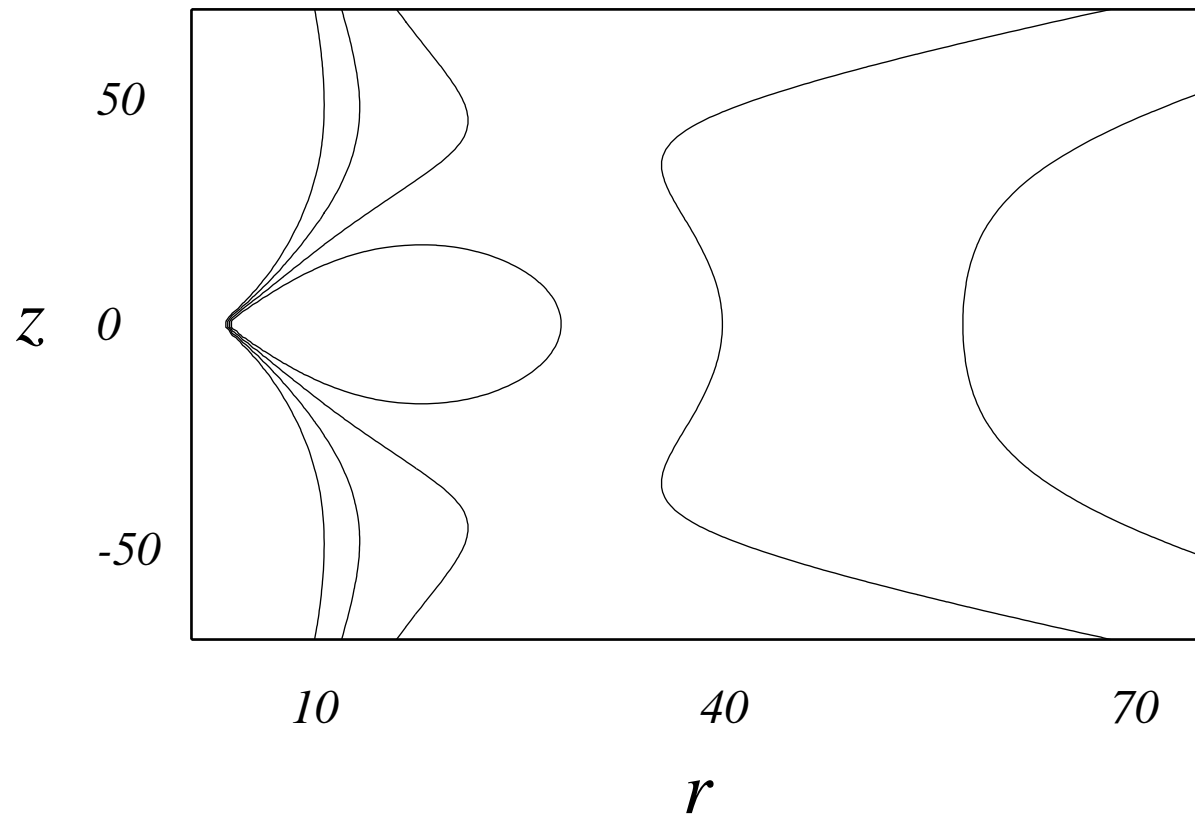


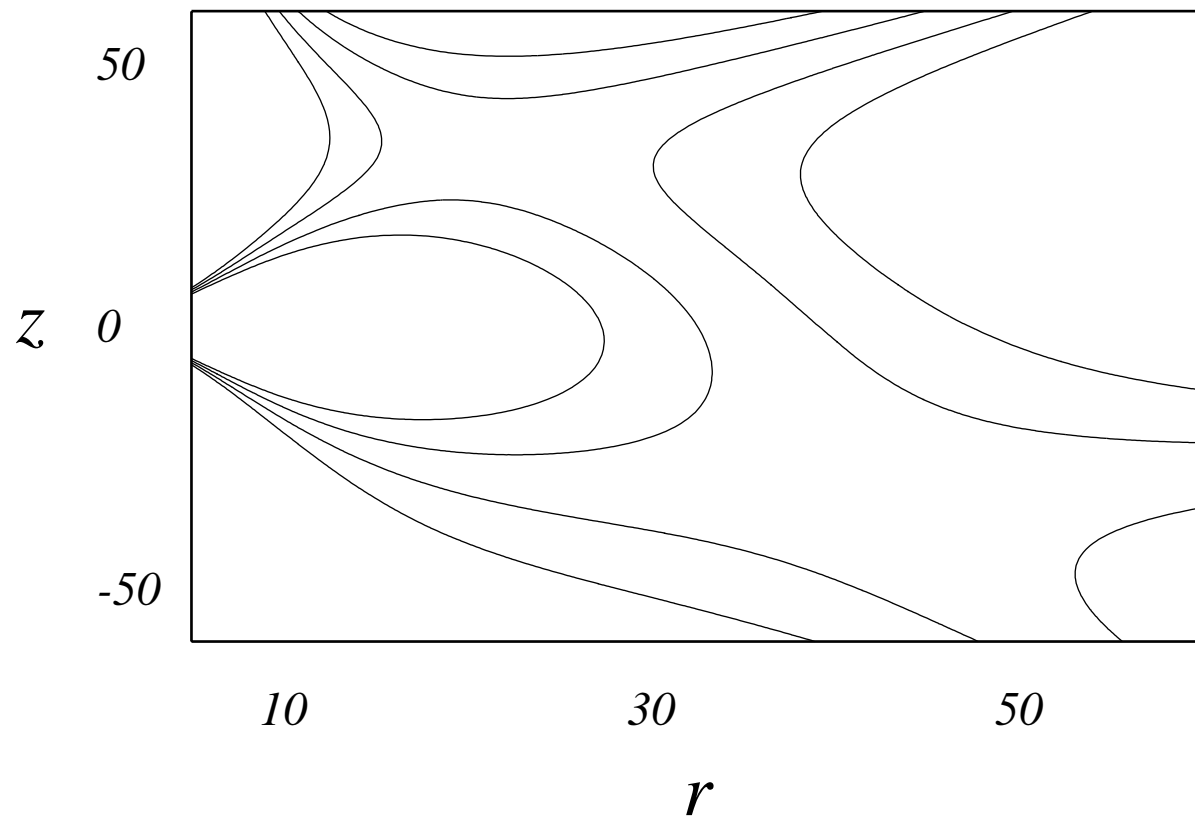


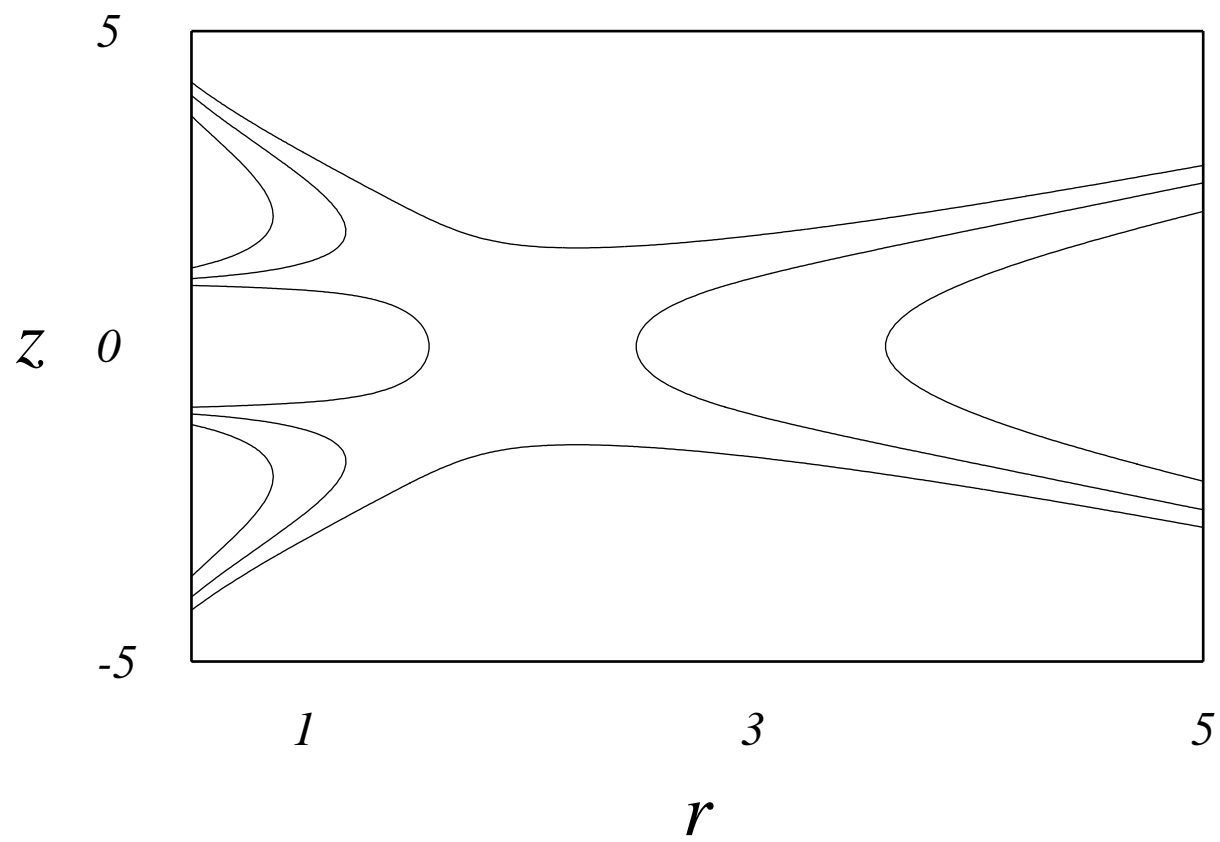


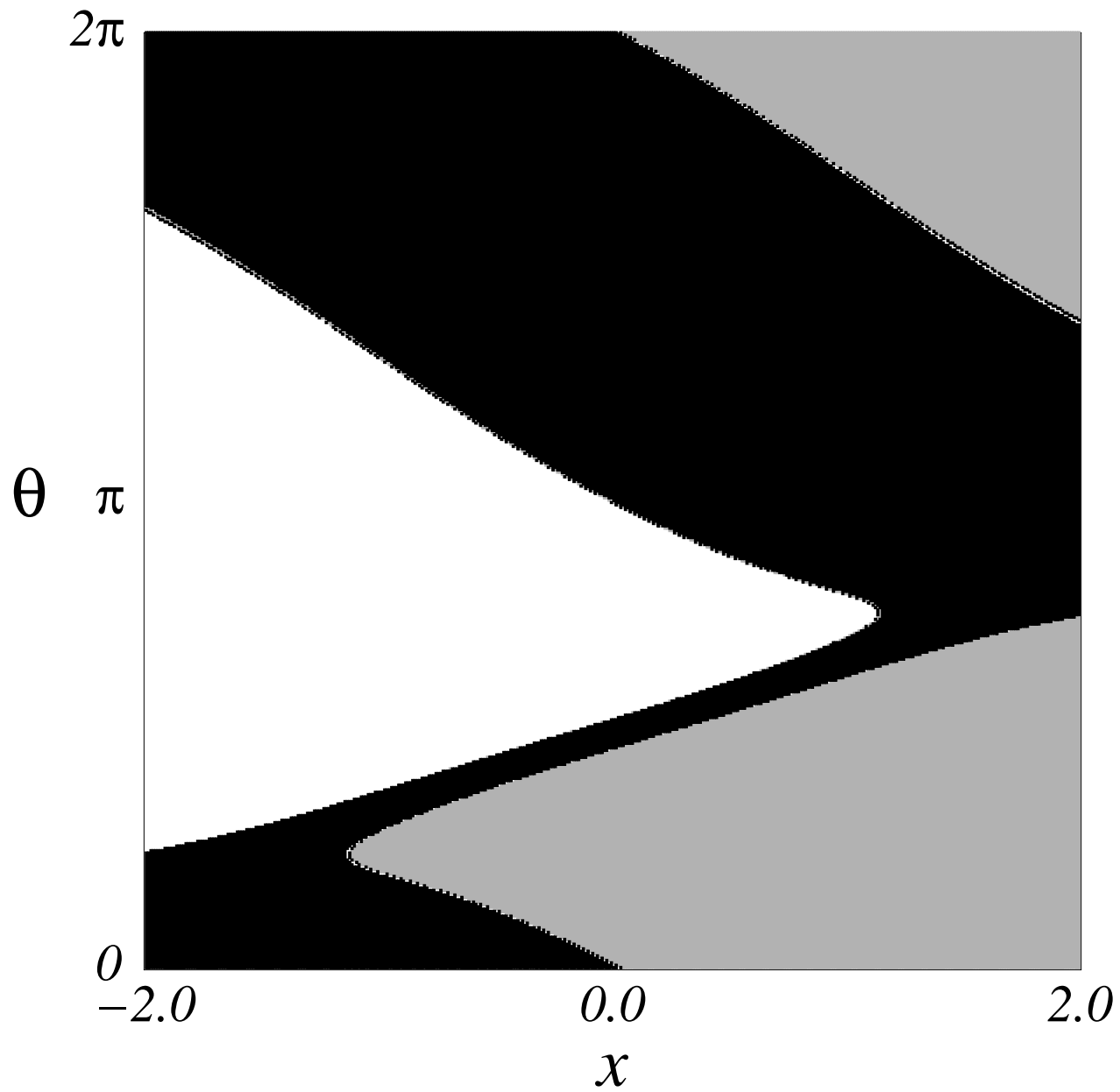












2.3878

θ

2.3873

1.14880

z

1.14888

